RSC Advances

PAPER

View Article Online
View Journal | View Issue

Cite this: *RSC Adv.*, 2026, **16**, 22600

Mutation of active site glutamate in serine hydroxymethyltransferase allows trapping a reactive intermediate: a combined neutron and X-ray crystallography study

Victoria N. Drago,[a] Robert S. Phillips [bc] and Andrey Kovalevsky *[a]

Serine hydroxymethyltransferase (SHMT) is a pyridoxal-5′-phosphate (PLP) dependent enzyme that catalyzes a chemical transformation essential for the one-carbon (1C) metabolism. SHMT reversibly converts L-Ser into Gly and transfers a 1C unit to tetrahydrofolate (THF) to give 5,10-methylene-THF (5,10-MTHF). 5,10-MTHF, a 1C-unit donor, plays a crucial role in the downstream biomolecular syntheses required for the cell homeostasis and proliferation. SHMT is a prominent target for the drug discovery to battle bacterial and parasitic infections, and to treat various types of cancer. SHMT-catalyzed chemistry is governed by the general acid-base catalysis. Knowledge of the catalytic mechanism can aid drug design but can only be achieved when the atomic details of each reaction step are mapped, including accurate determination of hydrogen atom positions. Here we utilized the inactive E53Q mutant of *Thermus thermophilus* (*Tth*) SHMT to directly determine protonation states with room-temperature neutron crystallography and to capture a reactive intermediate containing the PLP-L-Ser external aldimine and THF in the enzyme active site. We observed protonation of the Schiff base nitrogen (N_{SB}) in the PLP internal aldimine but no change in the protonation states of other ionizable PLP groups and active site residues compared to wild-type *Tth*SHMT. X-ray structural analysis of the ternary intermediate complex E53Q-Ser-THF that eluded previous structural characterization shows the strategic positioning of the E53Q side chain in close proximity to the external aldimine and THF and reinforces the proposed role for E53 as the driver of proton transfer events along the reaction pathway.

Received 2nd March 2026
Accepted 15th April 2026

DOI: 10.1039/d6ra01814a

rsc.li/rsc-advances

Introduction

Serine hydroxymethyltransferase (SHMT), an enzyme at the forefront of the one-carbon (1C) metabolic pathway, is a fold-type I pyridoxal-5′-phosphate-dependent enzyme responsible for the production of 5,10-methylene-tetrahydrofolate (5,10-MTHF), which is a reactive 1C-donating biomolecule. SHMT accomplishes the synthesis of 5,10-MTHF by converting L-serine into glycine and a concurrent transfer of the 1C unit (*i.e.* Cβ of L-Ser) to tetrahydrofolate (THF) in the THF-dependent reaction[1–3] (Fig. 1). Recently, it has been shown that SHMT also possesses THF-dependent dehydratase activity on D-serine, that is degraded into pyruvate and ammonia.[4,5] In addition, SHMT can catalyze the retro-aldol cleavage of some β-hydroxy amino acids, decarboxylation of aminomalonate, and racemization and transamination of L- and D-alanine in a THF-independent manner.[6,7] Downstream of SHMT along the 1C metabolic pathway, 5,10-MTHF is utilized by thymidylate synthase to directly transfer the 1C unit to deoxyuridine monophosphate (dUMP) to make deoxythymidine monophosphate (dTMP),[8] by a methylenetetrahydrofolate reductase to synthesize 5-methyl-THF,[9] and by a methylenetetrahydrofolate dehydrogenase to create 5-formyl-THF.[10] These metabolic products (Fig. 1) are critical for the subsequent biosyntheses of DNA, methionine, S-adenosylmethionine, formyl-methionyl-tRNA, and other essential biomolecules.[11–13] Recent advances in our understanding of SHMT's vital role in cell homeostasis and proliferation have propelled it to become a prominent target for the discovery of novel small-molecule antibacterial, antiparasitic, and anti-cancer drugs.[13–19]

To advance the design of SHMT inhibitors, including mechanism-based compounds, understanding SHMT catalysis at the atomic level is of paramount importance. The SHMT catalytic mechanism has been debated for over 40 years,[1,20–23] with a number of mechanisms proposed. No consensus has been reached, however, mainly due to the inability of the biophysical methods employed, such as X-ray crystallography, to determine the positions and movement of hydrogen (H)

[a]*Neutron Scattering Division, Oak Ridge National Laboratory, Oak Ridge, TN, 37831, USA. E-mail: kovalevskyay@ornl.gov*

[b]*Department of Chemistry, University of Georgia, Athens, GA, 30602, USA*

[c]*Department of Biochemistry and Molecular Biology, University of Georgia, Athens, GA, 30602, USA*

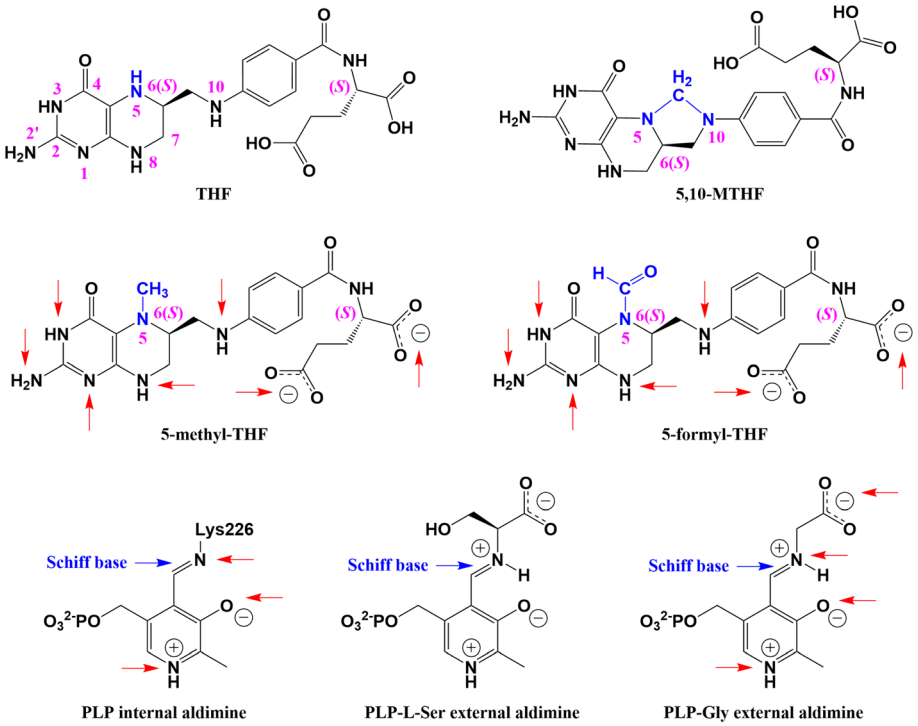

Fig. 1 Chemical diagrams of THF and its metabolic derivatives, PLP in its internal and L-Ser and Gly external aldimine forms. Only 6(*S*) diastereomers of THF and its derivatives bind to the SHMT active site. Red arrows indicate chemical groups whose protonation states were determined in the wild-type *Tth*SHMT with neutron crystallography.

atoms, which led to contradictory results from computational studies.[24–26] H atoms are key players in the general acid-base catalysis that governs SHMT function. H atom positions define the protonation states and establish the electrical charges on specific chemical groups, thus controlling the active site electrostatic environment and thereby directing enzyme catalysis. Neutron crystallography[27,28] is a powerful technique capable of pinpointing positions of functional H atoms involved in enzyme-driven proton transfers and labile H atoms that can move upon changes in the chemical and electrostatic environment inside the active site, and also accurately orienting and visualizing water species.[29–32] The reason neutron crystallography can directly determine locations of H atoms in a biological macromolecule at resolutions as low as 2.5–2.6 Å[33–35] is due to the fundamental scattering properties of neutrons. Neutrons are scattered by the atomic nuclei rather than by electron clouds that scatter X-rays, resulting in the atomic neutron scattering power being independent of the atomic number (https://www.ncnr.nist.gov/resources/n-lengths). H and its heavier isotope deuterium (D) scatter neutrons as well as C, N, and O. In addition, the cold neutrons with wavelengths of 1–5 Å, utilized in macromolecular crystallography, are nonionizing and do not induce radiation damage in crystals. This allows neutron diffraction data collection to be carried out at near-physiological (room) temperature.

We have been employing room-temperature neutron crystallography to investigate the catalytic mechanism in a bacterial SHMT from *Thermus thermophilus* (*Tth*SHMT, Fig. 2A). *Tth*SHMT is used as a model enzyme for the human mitochondrial SHMT2 (hSHMT2), because the active sites of the two proteins are conserved.[36–38] We have previously obtained five neutron structures of *Tth*SHMT, capturing the enzyme at various stages of its catalytic process, including (1) the *apo*-form that lacks the pyridoxal-5′-phosphate (PLP) coenzyme entirely, (2) the holoenzyme with PLP bound to the catalytic K226 in the internal aldimine form, (3) a *pre*-Michaelis complex with L-serine (L-Ser) coordinated at the peripheral binding site, (4) a complex with folinic acid mimicking the carbinolamine-THF intermediate, and (5) a ternary complex containing PLP-glycine (PLP-Gly) external aldimine and 5-methyl-THF (Fig. 1). Nuclear density maps revealed the positions of all exchangeable H atoms, provided accurate assignments of the protonation states and permitted us to propose a catalytic mechanism for both stages of the reaction – the initial conversion of the PLP internal aldimine into the external aldimine upon L-Ser attack on the Schiff base and the transfer of L-Ser Cβ-OH to THF with its subsequent dehydration leading to the product 5,10-MTHF (Fig. S1). In short, during the first stage, L-Ser substrate enters the active site as a zwitterion, with its amino group protonated and carboxyl group deprotonated. L-Ser initially binds at the peripheral binding site and the gating loop consisting of residues 342–356 in *Tth*SHMT is in the open conformation (Fig. 2B). L-Ser then moves deeper into the active site interior and binds at the cationic binding site near PLP. To become a reactive amine, the L-Ser N-terminus protonates the neutral Schiff base and subsequently attacks the Schiff base C4′, resulting in the PLP-L-Ser external aldimine formation through the transaldimination reaction. In the next stage, THF binds to the peripheral binding

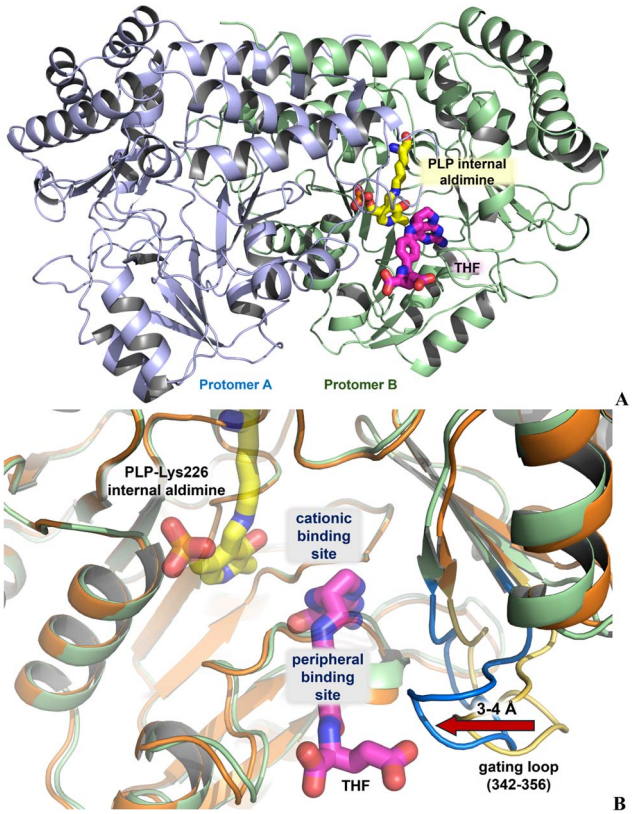

Fig. 2 Three-dimensional structure of *Tth*SHMT wild-type in complex with THF. (A) Homodimeric *Tth*SHMT in cartoon representation. PLP internal aldimine and bound THF are shown as sticks in protomer B (PDB ID 9O50). (B) Superposition of *Tth*SHMT-THF complex and the enzyme's apo-form (PDB ID 9O5G) highlighting the locations of the substrate binding sites and the gating loop motion upon THF binding.

site and its position is secured by the gating loop closure. The L-Ser Cβ-OH group is transferred to THF *via* a direct attack by the THF's N5 activated through its deprotonation by the catalytic glutamate (E53 in *Tth*SHMT). The result is the formation of the THF carbinolamine and the PLP quinonoid intermediates. The carbinolamine is dehydrated when a proton is transferred from the protonated E53 to its OH group, converting this intermediate into the THF N5-iminium cation. The iminium intermediate is cyclized to give the product 5,10-MTHF through the N10 attack on CH_2 after N10 is deprotonated by E53. Concurrently, the PLP quinonoid intermediate is converted into the PLP-Gly external aldimine by K226 protonating the PLP-Gly Cα. The PLP internal aldimine is regenerated through a trans-aldimination reaction utilizing the K226 side-chain amine, similar to the reaction involving L-Ser, to give the product Gly. Thus, in our proposal E53 acts as a universal acid-base catalyst in the direct displacement mechanism for the THF-dependent reaction catalyzed by SHMT,[37] unlike in previously proposed catalytic mechanisms that suggested involvement of several different residues.[20,23,24,39]

A crucial role of a catalytic glutamate in the THF-dependent catalysis of SHMT has been reported previously. It was shown that mutation E74Q in sheep liver cytosolic SHMT (scSHMT) and E75Q in rabbit liver cytosolic SHMT (rcSHMT) enzymes reduced the 5,10-MTHF production by 400–500 times, whereas E75L substitution in rcSHMT completely abolished the THF-dependent catalysis.[39,40] Interestingly, in a bacterial SHMT from *Bacillus stearothermophilus* (bsSHMT) mutation of the conserved glutamate to glutamine (E53Q) inactivated the enzyme completely,[41] in agreement with its proposed role as the general acid-base catalyst.[37] The location of the catalytic glutamate is identical in the *Tth*SHMT sequence to that in bsSHMT. We therefore aimed to map the H atom positions in the *Tth*SHMT E53Q mutant, compare them with the wild-type holoenzyme, and trap a reactive intermediate containing PLP-L-Ser external aldimine and THF. Here, we present a 2.4 Å resolution room-temperature neutron structure of the *Tth*SHMT E53Q holoenzyme containing the PLP-K226 linkage in its internal aldimine form. Moreover, we succeeded in trapping the E53Q mutant in a reactive complex with the PLP-L-Ser external aldimine and THF bound at the peripheral binding site, referred to as E53Q-Ser-THF henceforth, and obtained its room-temperature X-ray structure at 1.8 Å resolution. In the neutron structure of E53Q holoenzyme, we observed, for the first time in *Tth*SHMT, the protonated internal aldimine Schiff base, whereas the rest of the protonation states within the active site remained unchanged compared to the wild-type holoenzyme. In E53Q-Ser-THF, Q53, L-Ser Cβ-OH and THF's N5 and N10 are correctly juxtaposed for catalysis, but the lack of the general base necessary to deprotonate N5 due to E53Q mutation does not allow the reaction to proceed. The current neutron structure of *Tth*SHMT depicting protonation states in the E53Q holoenzyme and the X-ray structure of E53Q-Ser-THF complex reaffirm the critical role of the catalytic glutamate in the THF-dependent SHMT catalysis and show the active site preorganization required for the catalytic reaction.

Results

Protonation states in *Tth*SHMT E53Q and comparison with the wild-type holoenzyme

To map the protonation states in the active site of *Tth*SHMT E53Q we obtained the room-temperature neutron structure of this inactive mutant holoenzyme at 2.4 Å resolution, jointly refined with the 1.65 Å room-temperature X-ray diffraction data collected from the same crystal. *Tth*SHMT E53Q crystals are monoclinic, having the space group of $P2_1$, with the unit cell identical to that of the wild-type enzyme.[36] The whole homodimer of the E53Q holoenzyme occupies the asymmetric unit and the active sites in protomers A and B are the same, including the protonation states. The neutron structure analysis given below, therefore, is based on the active site in protomer A, unless specified otherwise.

In the E53Q holoenzyme, PLP is covalently connected to Lys226 Nζ atom through the Schiff base linkage. The N1 pyridine nitrogen of PLP is protonated and positively charged (Fig. 3A). N1 is hydrogen bonded to the carboxylate side chain of Asp197 with the D···O and N···O distances of 1.8 and 2.6 Å, respectively. The Asp197 side chain position is secured by additional hydrogen bonds it makes with the side chains of Asn98 and His125, and with the Ala199 main chain. The O3′

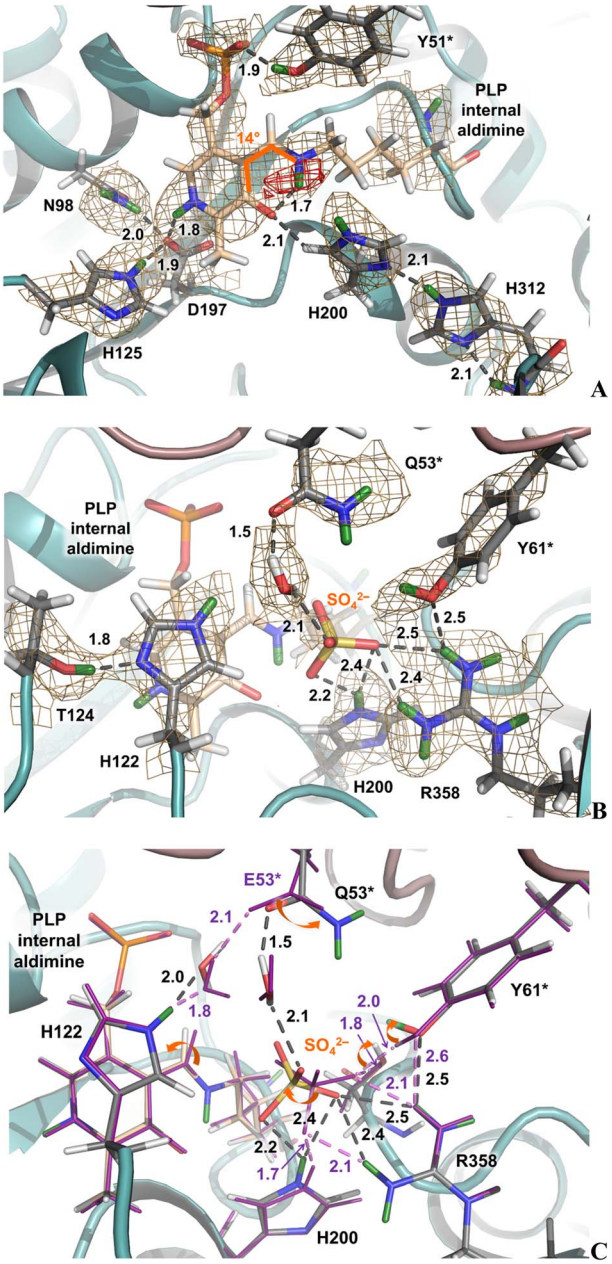

Fig. 3 Neutron scattering length density maps for the active site in *Tth*SHMT E53Q holoenzyme. The $2F_O-F_C$ map shown as light brown mesh is contoured at 1.2 σ level and omit F_O-F_C map in red mesh is contoured at 2.5 σ level. (A) PLP internal aldimine and surrounding residues. The out-of-plane rotation of the Schiff base is 14° depicted using orange sticks (the equivalent torsion angle in protomer B is 17°). (B) Binding of a sulfate anion and the mutation site. (C) Superposition of the wild-type (PDB ID 8SUJ) and E53Q mutant holoenzyme active sites. H atoms are colored white, and D atoms are green. Orange arrows indicate shifts and rotations of specific groups due to mutation. Distances are in Angstroms.

oxygen atom is in the deprotonated phenolate form. O3′ makes an unconventional C–H···O bond with Cδ2 of His200 imidazole (H···O and C···O distances of 2.1 and 3.0 Å, respectively). Such His200 orientation allows it to form a hydrogen bond with His312 having the D···N and N···N distances of 2.1 and 3.1 Å, respectively, and a bifurcated N–D···O hydrogen bond with SO_4^{2-} anion, with the D···O distances of 2.2 and 2.4 Å and N···O distances of 3.0 and 3.3 Å. His312 side chain rotation is controlled by the hydrogen bonds with its own main chain amide ND and with His200.

The Schiff base nitrogen N_{SB} of PLP was found to be protonated, hence, positively charged. The omit F_O-F_C neutron scattering length density map unambiguously demonstrates the presence of D on N_{SB} (Fig. 3A). Thus, N_{SB} gained a D atom in the E53Q mutant but was observed in the neutral (non-protonated) form in the PLP internal aldimine state of the wild-type holoenzyme and in complexes with L-Ser or folinic acid bound at the peripheral binding site.[36,37] The protonated N_{SB} was also detected in the PLP-Gly external aldimine structure of the wild-type enzyme, presumably protonated by the incoming zwitterionic Gly substrate.[38] The N_{SB}–D bond faces O3′ making a 1.7 Å hydrogen bond and creating a six-membered cycle that stabilizes the Schiff base position. The protonated C4′=N_{SB} double bond is 14° (protomer A) and 17° (protomer B) out of the pyridinium plane on the *si* face of PLP. The corresponding dihedral angles were measured at 29–38° for the neutral Schiff base of the PLP internal aldimine in our earlier neutron structures.[36,37] This observation is in agreement with our previous quantum-chemical calculations that showed the out-of-plane geometry of the neutral Schiff base is stabilized by hyperconjugation with

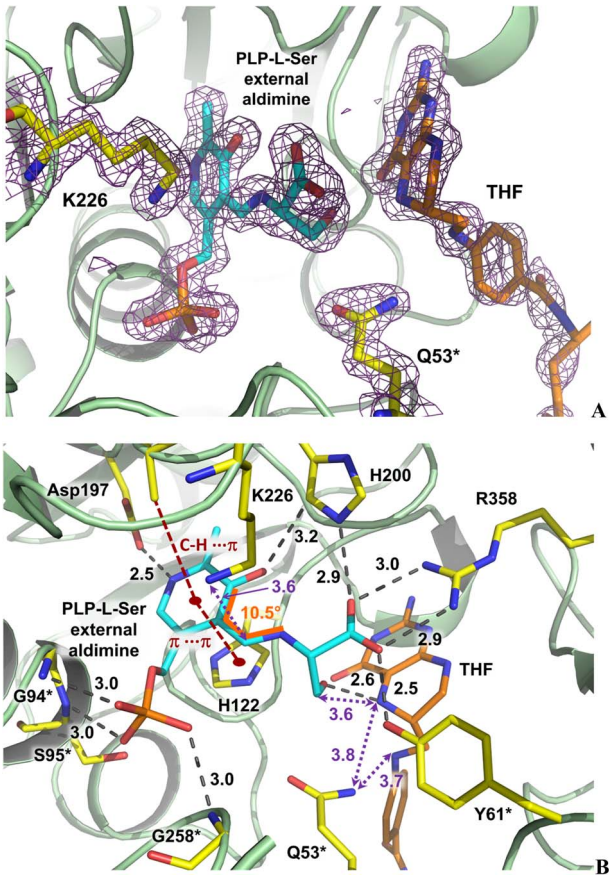

Fig. 4 Organization of the active site in protomer B of E53Q-Ser-THF complex. (A) The $2F_O-F_C$ electron density map is shown as violet mesh contoured at 1.4 σ level. (B) Interactions between PLP-L-Ser, THF and the active site residues. Distances are in Angstroms.

the pyridinium ring, whereas the N_{SB} protonation promotes the C4′=N_{SB} double bond rotation towards the pyridinium plane.[36,42]

In the current neutron structure of E53Q holoenzyme, a sulfate anion (SO_4^{2-}) is observed captured in the cationic binding site. The SO_4^{2-} anion position is stabilized by a favorable electrostatic interaction with the positively charged R358 guanidinium side chain (Fig. 3B and S2). The sulfate is further surrounded by H122, H200, Q53*, and Tyr61* (the asterisk indicates the residue belongs to protomer B) and makes a water-mediated interaction with Q53*. Importantly, the protonation states of all active site histidine residues, including H122, H125, H200, H225, and H312 (Fig. S3), remain neutral and identical tautomers with Nε2 nitrogen atoms protonated and Nδ1 not protonated, as was also observed in our previous neutron structures of *Tth*SHMT.[36–38]

The *Tth*SHMT wild-type and E53Q mutant holoenzyme neutron structures superimpose with the RMSD of 0.12 Å, implying the catalytic residue mutation did not perturb the overall enzyme structure, although small structural differences within the active site are possible. The positions of most active site residues are virtually identical, including the PLP internal aldimine except for the tilt of the Schiff base (Fig. 3C). One notable difference is at the mutation site where the Q53* side chain shifts and rotates away from where the E53* side chain was placed in the wild-type enzyme to lose a water-mediated contact with H122. The other difference is a slight 0.6 Å, but significant, shift and a 30° rotation of SO_4^{2-} anion away from R358, weakening the salt bridge hydrogen bonds. The sulfate movement also results in the breaking of hydrogen bonds with Y61* and S31 side chain hydroxyls that rotate by 45° and 51° in E53Q holoenzyme.

Active site pre-organization in the reactive E53Q-Ser-THF complex

To visualize the intermediate formed just before the L-Ser Cβ-OH hydroxymethylene group is transferred to the THF's N5 atom, we succeeded in determining a room-temperature X-ray structure of the *Tth*SHMT E53Q mutant ternary complex with L-Ser and THF at 1.8 Å resolution (Table S2). Interestingly, earlier attempts to obtain such a complex by using the inactive rcSHMT E75L mutant failed, with the electron density map found to be inadequate to determine what species were bound in the active site.[39] In the E53Q-Ser-THF complex, however, the electron density unequivocally showed the PLP-L-Ser external aldimine, the K226 side chain released from the starting internal aldimine, Q53, and THF at the peripheral binding side (Fig. 4A). As in our previous complexes of *Tth*SHMT,[37,38] the PLP-L-Ser external aldimine formation and THF binding occurred only in protomer B (Fig. S4), because the gating loop open-close dynamics required for the active site reactivity towards L-Ser and THF binding are hindered in protomer A due to crystal packing interactions. The electron density also reveals that only the C6-(*S*) diastereomer of THF is bound in E53Q-Ser-THF, as it does in the *Tth*SHMT/THF complex.[38]

In E53Q-Ser-THF, the PLP-L-Ser external aldimine is held in place by numerous conventional and nonconventional interactions (Fig. 4B). The pyridine nitrogen makes a short 2.5 Å hydrogen bond with D197, whereas the O3′ forms a nonconventional C–H···O hydrogen bond with H200. The C-terminal carboxylate of L-Ser takes advantage of all hydrogen bonding possibilities by forming a salt bridge with R358 and hydrogen bonds with Y61* and H200. Several hydrogen bonds made by the phosphate group with the main chain amides of G94*, S95* and G258* secure its position. In addition, the pyridine ring of PLP-L-Ser interacts by the π···π stacking and C–H···π contacts with the side chains of H122 and A199, respectively. The Schiff base in the external aldimine is rotated by −10.5° out of the pyridine plane, which is similar to the C4′ = N_{SB} out-of-plane torsion of −8° in *Tth*SHMT-Gly-5MTHF complex.[38] In both complexes the Schiff base rotates past the pyridine plane to the *re* face in the PLP-Gly external aldimine (Fig. S5). Such a PLP-L-Ser external aldimine conformation suggests protonation of N_{SB} as observed in the PLP-Gly external aldimine and ensures that the Cβ-OH group is close to THF's N5 making a 2.6 Å hydrogen bond. The K226 side chain amine is placed above the Schiff base as in the PLP-Gly external aldimine and its Nζ atom makes a 3.6 Å N–H···π contact with C4′ (Fig. 4B). Importantly for the catalytic mechanism, N5 is just 3.6 Å away from PLP-L-Ser Cβ and 3.8 Å away from Q53* side chain. Q53* also contacts Cβ, with the O···C distance of 3.2 Å, and is just 3.7 Å away from the THF's N10.

Discussion

H atoms are key players in general acid-base catalysis, as the catalytic reactions are facilitated through a series of proton transfers occurring in the enzyme active sites to convert substrates into products. In THF-dependent SHMT catalysis, which involves two substrates and a covalently bound coenzyme PLP, no fewer than ten proton transfer events must happen to convert the L-Ser and THF substrates into Gly and 5,10-MTHF products, respectively. Several neutron crystallographic studies[36–38] have revealed the protonation states of the PLP in both internal and external aldimine forms, active site residues, and THF analogues. These studies established E53 as the only residue capable of changing its protonation state along the reaction pathway – an observation only possible by neutron crystallography. Crucially for catalysis, E53 is strategically placed in close proximity to the reactive Cβ-OH group of the PLP-L-Ser and THF's N5 and N10 atoms. This led us to propose a direct displacement mechanism for the THF-dependent reaction catalyzed by the conserved glutamate (E53 in *Tth*SHMT and bsSHMT) acting as a universal acid-base catalyst, instead of by several different residues.[37] We therefore engineered the point mutation E53Q in *Tth*SHMT in order to study the inactive mutant's active site organization at the atomic level and to trap a reactive intermediate that eluded structural characterization previously.

Unsurprisingly, in the E53Q holoenzyme, the pyridine N1 atom of the PLP internal aldimine is protonated, thus positively charged, as it is hydrogen bonded to the Asp197 carboxylate,

a conserved residue in fold type I PLP-dependent enzymes (Fig. S6).[36,42–44] O3′ is observed as a deprotonated, negatively charged phenolate that engages in an unconventional C–H···O bond with the H200 imidazole. The O3′ protonation state is unchanged in previous wild-type *Tth*SHMT neutron structures,[36–38] and in aspartate aminotransferase (fold type I)[42,45] and tryptophan synthase (fold type II).[46] Five active-site histidines, His122, His125, His200, His225, and His312, create a histidine cage that encapsulates the PLP. All of these histidines are neutral in E53Q, with protonated Nε2 and non-protonated Nδ1, and their protonation states and tautomeric forms are invariant between various complexes and reaction intermediate mimics of wild-type *Tth*SHMT.[36–38] The neutron scattering length density map also revealed that the Schiff base N_{SB} is protonated in E53Q holoenzyme. This is the first time the protonated N_{SB} is observed for the PLP internal aldimine in *Tth*SHMT, suggesting the Schiff base protonation state can be finely tuned by the active site electrostatic environment. Computational studies will be required to support the proposed mechanism for SHMT catalysis[37] that involves protonation of the Schiff base by an incoming amino acid substrate.

Addition of L-Ser and THF to E53Q mutant enzyme resulted in the formation of the PLP-L-Ser external aldimine and THF binding at the peripheral binding site to give a ternary E53Q-Ser-THF complex. E53Q-Ser-THF is a reactive complex with the PLP-L-Ser Cβ-OH group poised for transfer to THF's N5 when the nitrogen is deprotonated. This complex eluded structural analysis as previous attempts failed to generate interpretable electron density maps using mutant bsSHMT.[39] In the current E53Q-Ser-THF room temperature X-ray structure, the electron density is unambiguous for the PLP-L-Ser external aldimine and THF, showing preorganization of the active site for catalysis. The Q53 side chain is naturally not capable of carrying out the necessary proton transfers for catalysis to ensue, but its position in relation to the external aldimine and THF would indicate that, in the actual catalytic E53-Ser-THF complex, the glutamate would be able to execute catalysis.

Conclusion

By using neutron protein crystallography at near-physiological (room) temperature we visualized the protonation states in the inactive E53Q mutant of *Tth*SHMT holoenzyme. The PLP internal aldimine is protonated at both pyridine N1 and Schiff base N_{SB} atoms, having the $C4' = N_{SB}$ bond rotated closer to the pyridine plane than in the wild-type holoenzyme. As in all neutron structures of *Tth*SHMT, the active site His residues are neutral, suggesting their protonation states conservation is important for creating a specific electrostatic environment for catalysis. We also succeeded in determining a room-temperature X-ray structure of the elusive substrate–bound complex containing PLP-L-Ser external aldimine and THF. Structural analysis of this complex reinforces the proposed role for E53 as the general acid-base catalyst that drives the proton transfer events along the reaction pathway. *Tth*SHMT E53Q is a useful model system for further neutron diffraction studies of the catalytic mechanism, including for hSHMT2, and can be utilized in the neutron structure-assisted design of SHMT inhibitors.

Methods

General information

Columns for protein purification were purchased from Cytiva (Piscataway, New Jersey, USA). His-tagged Tobacco Etch Virus (TEV) protease was produced in-house. Crystallization reagents and supplies were purchased from Hampton Research (Aliso Viejo, California, USA). Crystallographic supplies for crystal mounting and X-ray and neutron diffraction data collection at room temperature were purchased from MiTeGen (Ithaca, New York, USA) and Vitrocom (Mountain Lakes, New Jersey, USA). L-Ser (cat. no. S4500) and THF (a mixture of diastereomers, cat. no. T3125) were purchased from Millipore Sigma (St. Louis, Montana, USA).

Expression and purification. A detailed procedure for the expression and purification of *Tth*SHMT was published elsewhere.[36,37] The kanamycin-resistant pJ411 plasmid (ATUM, Newark, CA) encoding *Tth*SHMT E53Q variant and an N-terminal linker containing a His_6-tag, a 34 amino acid long linker sequence and a TEV protease cleavage site ENLYFQS was transformed into the *E.coli* BL21(DE3) expression vector. The cells were grown in Luria–Bertani (LB) media with 50 μg mL^{-1} kanamycin at 37 °C to an optical density (OD) of 0.8–1.0. For protein expression, the cell cultures were induced with 1 mM isopropyl ß-D-1-thiogalactopyranoside (IPTG) and maintained overnight at 22 °C in a shaker. After centrifugation the next day, the cell pellets were resuspended in the lysis buffer made with 50 mM sodium phosphate pH 7.5, 500 mM NaCl, and 10 mM imidazole at a ratio of 5 mL of the buffer per gram of wet cell paste. Lysozyme was added to the resuspended cells at a concentration of 0.1 mg mL^{-1} and stirred on ice for 30 min before the cells were disrupted by sonication. The lysate was clarified by centrifugation at 30 000 *g* to remove the insoluble fraction. The His-tagged *Tth*SHMT E53Q was purified *via* affinity chromatography using a HisTrapFF (5 mL) nickel column equilibrated with 20 mM HEPES pH 7.5, 100 mM NaCl, and 10 mM imidazole. The protein was eluted from the column using a linear gradient of 20 mM HEPES pH 7.5, 100 mM NaCl, and 500 mM imidazole. TEV protease (1 mg TEV protease/100 mg of tagged protein) was added to purified *Tth*SHMT E53Q and the mixture was dialyzed against 20 mM HEPES pH 7.5, 100 mM NaCl, and 1 mM EDTA overnight at room temperature. The resultant solution was loaded onto a HisTrapFF (5 mL) nickel column and untagged *Tth*SHMT E53Q was collected in the flow-through. Pure *Tth*SHMT E53Q was dialyzed against 40 mM NaOAc pH 5.4 and 1 mM PLP to ensure all enzyme molecules contained active sites with bound PLP in internal aldimine form and concentrated to ~20 mg mL^{-1}. For long-term storage at −30 °C, glycerol was added to the concentrated protein up to the concentration of 20% (v/v) as a cryoprotectant to avoid the protein crashing out of the solution upon thawing.

Crystallization, soaking, and H/D-exchange. For crystallization experiments, frozen *Tth*SHMT E53Q was thawed and

dialyzed overnight against 40 mM NaOAc pH 5.4 and 1 mM PLP to remove the cryoprotectant. The protein was then crystallized by sitting drop vapor diffusion methodology using 40 mM NaOAc pH 5.5, 1 M $(NH_4)_2SO_4$, and 0.5 M Li_2SO_4 as the precipitant solution at 16 °C. To obtain large crystals crystallization drops were microseeded with a seeding tool from Hampton Research in 9-well glass plates and sandwich box setups using microseeds obtained by crushing previously crystallized aggregates. A large crystal of *Tth*SHMT E53Q was mounted in a 2 mm-inner diameter quartz capillary containing a liquid plug made of 40 mM NaOAc pH 5.5, 1 M $(NH_4)_2SO_4$, and 0.5 M Li_2SO_4 in 99.8% D_2O to perform H/D-vapor exchange. Because THF does not bind to *Tth*SHMT in high concentrations of salt, the E53Q-Ser-THF complex was made in the following way. A crystal of *Tth*SHMT E53Q holoenzyme was transferred to a fresh drop containing 40 mM NaOAc pH 5.5 and 15% PEG 4000 and soaked overnight to remove most of sulfate. The crystal was then moved into another drop containing a soaking solution with 40 mM NaOAc pH 5.5, 15% PEG 4000, 0.5 M L-Ser and 10 mM THF on the next day, and the crystal was kept in this solution overnight before harvesting it for room-temperature X-ray crystallography.

X-ray diffraction data collection and structure refinement. Room temperature X-ray diffraction data collection on *Tth*SHMT E53Q holoenzyme and E53Q-Ser-THF complex crystals were performed on a Rigaku HighFlux HomeLab instrument equipped with a MicroMax-007 HF X-ray generator, Osmic VariMax optics, and a DECTRIS Eiger R 4 M detector at ORNL. The data were indexed and integrated using the CrysAlisPro software package (Rigaku, The Woodlands, TX), and the data were reduced and scaled in the AIMLESS program in the CCP4 software suite.[47,48] The X-ray structures were solved by molecular replacement in PHASER[49] using phases from PDB code 8SUJ and refined with phenix.refine in the PHENIX suite.[50,51] The room temperature X-ray structure of *Tth*SHMT E53Q holoenzyme was subsequently used in joint X-ray/neutron refinement. Ligand restraints for PLP internal aldimine, PLP-L-Ser external aldimine and THF were generated with eLBOW[52] using geometry optimized by quantum chemical calculations in Gaussian16[53] at B3LYP/6–31 g(d,p) level of theory. The X-ray diffraction data collection statistics are presented in Tables S1 and S2.

Neutron diffraction data collection. Neutron diffraction was first tested at room temperature on the IMAGINE[54–56] instrument located at the High Flux Isotope Reactor (Oak Ridge National Laboratory) using the broad bandpass functionality with neutron wavelengths between 2.8 and 10 Å. The neutron diffraction quality from the 0.5 mm^3 crystal was considered sufficient for a full data collection using the quasi-Laue diffraction mode of IMAGINE with the neutron wavelength range of 2.8–4.5 Å. The diffraction data extended to 2.4 Å resolution. Each neutron image exposure was 24 h, and the crystal was held in a stationary position. The crystal was rotated along the vertical axis ($\Delta\varphi = 8°$) before collecting each successive image. The crystal orientation was changed two times by tilting the capillary with respect to the incident neutron beam to improve data completeness. In total, 32 neutron diffraction images were collected. Neutron diffraction data processing was performed with a version of LAUEGEN[57,58] modified to account for the geometry of the cylindrical image plate detector. The wavelength–normalization curve was determined using the intensities of symmetry-equivalent reflections at different wavelengths in LSCALE.[59] No explicit absorption corrections were applied. The data were scaled and merged in SCALA.[60] Neutron data collection statistics can be found in Table S1.

Joint X-ray/neutron (XN) refinement. Joint XN refinement of the *Tth*SHMT E53Q holoenzyme was carried out using nCNS,[61,62] a patch of the Crystallography & NMR Systems (CNS)[63] software suite in the same manner as for our previous *Tth*SHMT structures.[36–38] A single rigid body refinement was the first step in the refinement procedure. Several separate rounds of the atomic position, atomic displacement parameter, and D atom occupancy refinements followed. In between the rounds of the joint XN refinement, the structure was visualized in the molecular graphics program COOT[64] to confirm correct side chain modeling and direct the rotation of side chain hydroxyl, thiol, and ammonium groups as well as water molecules to construct accurate hydrogen bonding networks. Water molecules were modeled and refined as D_2O due to H/D-vapor exchange. The enzyme molecule was modeled with H atoms at non-exchangeable positions because hydrogenated protein was used in the experiment, while labile (exchangeable) positions were modeled as D atoms. After D atom occupancy refinement, the exchangeable sites were modeled based on individual site occupancies, where an occupancy of −0.56 is indicative of a pure H atom and an occupancy of 1.00 reflects a pure D atom. Sites partially occupied by both H and D atoms were given two atom records with the partial occupancies adding up to 1.00. The percentage of D atom occupancy at a specific site is calculated according to the following formula: % D = (occupancy(D) + 0.56)/1.56. Joint X-ray/neutron refinement statistics can be found in Table S1.

Author contributions

V. N. D., R. S. P. and A. K. designed the study. V. N. D. expressed, purified and crystallized the protein. V. N. D. and A. K. collected and reduced X-ray and neutron diffraction data and refined the structures. V. N. D., R. S. P., and A. K. wrote the paper.

Conflicts of interest

There are no conflicts of interest to declare.

Abbreviations

Tth	*Thermus thermophilus*
SHMT	Serine hydroxymethyltransferase
THF	Tetrahydrofolate
5,10-MTHF	5,10-Methylene-tetrahydrofolate
5MTHF	5-Methyl-tetrahydrofolate

hSHMT2	human mitochondrial serine hydroxymethyltransferase
PLP	Pyridoxal-5′-phosphate

Data availability

The data supporting this article have been included as part of the supplementary information (SI). Supplementary information: Table S1, Fig. S1–S6. See DOI: https://doi.org/10.1039/d6ra01814a.

Crystallographic data for *Tth*SHMT E53Q and E53Q-Ser-THF have been deposited at the PDB under accession codes 10 YN and 10 ZB, respectively and can be obtained from https://doi.org/10.2210/pdb10YN/pdb and https://doi.org/10.2210/pdb10ZB/pdb.

Acknowledgements

A portion of this research used resources at the High Flux Isotope Reactor (HFIR), a DOE Office of Science User Facility operated by the Oak Ridge National Laboratory (ORNL). The beam time was allocated to IMAGINE instrument on proposal number IPTS-31466. The Office of Biological and Environmental Research supported a portion of this research that used resources at ORNL's Center for Structural Molecular Biology (CSMB), a DOE Office of Science User Facility. ORNL is managed by UT-Battelle LLC for DOE's Office of Science, the single largest supporter of basic research in the physical sciences in the United States. This research was supported by a grant from NIH-GMS (R01GM137008) to R.S.P. and A.K.

References

1 L. Schirch, Serine hydroxymethyltransferase, *Adv. Enzymol. Relat. Areas Mol. Biol.*, 1982, **53**, 83–112.
2 R. Percudani and A. Peracchi, A genomic overview of pyridoxal-phosphate-dependent enzymes, *EMBO Rep.*, 2003, **4**, 850–854.
3 R. Florio, M. L. di Salvo, M. Vivoli and R. Contestabile, Serine hydroxymethyltransferase: a model enzyme for mechanistic, structural, and evolutionary studies, *Biochim. Biophys. Acta*, 2011, **1814**, 1489–1496.
4 T. Miyamoto, S. Fushinobu, Y. Saitoh, M. Sekine, M. Katane, K. Sakai-Kato and H. Homma, Novel tetrahydrofolate-dependent D-serine dehydratase activity of serine hydroxymethyltransferase, *FEBS J.*, 2024, **291**, 308–322.
5 M. Hayashi, K. Sakai-Kato and T. Miyamoto, Multifunctionality analysis of serine hydroxymethyltransferases from human and Escherichia coli, *Biochim. Biophys. Acta, Proteins Proteomics*, 2026, **1874**, 141107.
6 K. Shostak and V. Schirch, Serine hydroxymethyltransferase: mechanism of the racemization and transamination of D- and L-alanine, *Biochemistry*, 1988, **27**, 8007–8014.
7 Y. Chiba, T. Terada, M. Kameya, K. Shimizu, H. Arai, M. Ishii and Y. Igarashi, Mechanism for folate-independent aldolase reaction catalyzed by serine hydroxymethyltransferase, *FEBS J.*, 2012, **279**, 504–511.
8 M. P. Costi, S. Ferrari, A. Venturelli, S. Calo, D. Tondi and D. Barlocco, Thymidylate synthase structure, function and implication in drug discovery, *Curr. Med. Chem.*, 2005, **12**, 2241–2258.
9 E. E. Trimmer, Methylenetetrahydrofolate reductase: biochemical characterization and medical significance, *Curr. Pharm. Des.*, 2013, **19**, 2574–2593.
10 L. N. Zhao and P. Kaldis, The catalytic mechanism of the mitochondrial methylenetetrahydrofolate dehydrogenase/cyclohydrolase (MTHFD2), *PLoS Comput. Biol.*, 2022, **18**, e1010140.
11 K. Herbig, E. P. Chiang, L. R. Lee, J. Hills, B. Shane and P. J. Stover, Cytoplasmic serine hydroxymethyltransferase mediates competition between folate-dependent deoxyribonucleotide and S-adenosylmethionine biosyntheses, *J. Biol. Chem.*, 2002, **277**, 38381–38389.
12 B. Petrova, A. G. Maynard, P. Wang and N. Kanarek, Regulatory mechanisms of one-carbon metabolism enzymes, *J. Biol. Chem.*, 2023, **299**, 105457.
13 J. Zhang, S. E. Lee, J. Yoon, B. J. Ku, J. O. Park, D. H. Kang, J. Y. Heo and Y. E. Kang, Multifaceted role of serine hydroxymethyltransferase in health and disease, *Mol. Cells*, 2025, **48**, 100262.
14 C. R. Cuthbertson, Z. Arabzada, A. 3rd Bankhead, A. Kyani and N. Neamati, A Review of Small-Molecule Inhibitors of One-Carbon Enzymes: SHMT2 and MTHFD2 in the Spotlight, *ACS Pharmacol. Transl. Sci.*, 2021, **4**, 624–646.
15 Y. Makino, C. Oe, K. Iwama, S. Suzuki, A. Nishiyama, K. Hasegawa, H. Okuda, K. Hirata, M. Ueno, K. Kawaji, M. Sasano, E. Usui, T. Hosaka, Y. Yabuki, M. Shirouzu, M. Katsumi, K. Murayama, H. Hayashi and E. N. Kodama, Serine hydroxymethyltransferase as a potential target of antibacterial agents acting synergistically with one-carbon metabolism-related inhibitors, *Commun. Biol.*, 2022, **5**, 619.
16 M. J. Nayeen, J. M. Katinas, T. Magdum, K. Shah, J. E. Wong, C. E. O'Connor, A. N. Fifer, A. Wallace-Povirk, Z. Hou, L. H. Matherly, I. I. I. C. E. Dann and A. Gangjee, Structure-Based Design of Transport-Specific Multitargeted One-Carbon Metabolism Inhibitors in Cytosol and Mitochondria, *J. Med. Chem.*, 2023, **66**, 11294–11323.
17 P. Mee-udorn, K. Phiwkaow, R. Tinikul, K. Sanachai, S. Maenpuen and T. Rungrotmongkol, In silico and in vitro potential of FDA-approved drugs for antimalarial drug repurposing against Plasmodium serine hydroxymethyltransferase, *ACS Omega*, 2023, **8**, 35580–35591.
18 R. Fu, F. Sun, W. Wang, R. Wang, H. Zhang, X. He, A. Liu and L. Yang, SHMT proteins: an emerging set of serine hydroxymethyltransferase in cancer, *Cell. Signal.*, 2025, **135**, 111977.
19 S. Zhu, Y. Liu, H. Chen, X. Zhu, X. Liu, K. Xu, Y. Sang, L. Shang, W. Chong and L. Li, Mechanism and therapeutic progress of one-carbon metabolic key enzyme: serine hydroxymethyltransferase 2 in cancer, *Clin. Med. Insights:Oncol.*, 2025, **19**, 1–14.

20 R. G. Matthews and J. T. Drummond, Providing One-Carbon Units for Biological Methylations - Mechanistic Studies on Serine Hydroxymethyltransferase, Methylenetetrahydrofolate Reductase, and Methyltetrahydrofolate-Homocysteine Methyltransferase, *Chem. Rev.*, 1990, **90**, 1275–1290.

21 V. Schirch, K. Shostak, M. Zamora and M. Gautam-Basak, The origin of reaction specificity in serine hydroxymethyltransferase, *J. Biol. Chem.*, 1991, **266**, 759–764.

22 J. R. Jagath, B. Sharma, N. A. Rao and H. S. Savithri, The role of His-134, -147, and -150 residues in subunit assembly, cofactor binding, and catalysis of sheep liver cytosolic serine hydroxymethyltransferase, *J. Biol. Chem.*, 1997, **272**, 24355–24362.

23 V. Schirch and D. M. Szebenyi, Serine hydroxymethyltransferase revisited, *Curr. Opin. Chem. Biol.*, 2005, **9**, 482–487.

24 H. S. Fernandes and M. J. Ramos, Cerqueira NMFSA Catalytic Mechanism of the Serine Hydroxymethyltransferase: A Computational ONIOM QM/MM Study, *ACS Catal.*, 2018, **8**, 10096–10110.

25 J. Santatiwongchai, D. Gleeson and M. P. Gleeson, Theoretical evaluation of the reaction mechanism of serine hydroxymethyltransferase, *J. Phys. Chem. B*, 2019, **123**, 407–418.

26 K. Soniya and A. Chandra, Free energy landscape and proton transfer pathways of the trasnimination reaction at the active site of the serine hydroxymethyltransferase enzyme in aqueous medium, *J. Phys. Chem. B*, 2021, **125**, 11848–11856.

27 M. P. Blakeley and A. D. Podjarny, Neutron macromolecular crystallography, *Emerg. Top. Life Sci.*, 2018, **2**, 39–55.

28 F. Kono, K. Kurihara and T. Tamada, Current status of neutron crystallography in structural biology, *Biophys. Physicobiol.*, 2022, **19**, e190009.

29 T. P. Halsted, K. Yamashita, C. C. Gopalasingam, R. T. Shenoy, K. Hirata, H. Ago, G. Ueno, M. P. Blakeley, R. R. Eady, S. V. Antonyuk, M. Yamamoto and S. S. Hasnain, Catalytically important damage-free structures of a copper nitrite reductase obtained by femtosecond X-ray laser and room-temperature neutron crystallography, *IUCrJ*, 2019, **6**, 761–772.

30 H. Kwon, J. Basran, J. M. Devos, R. Suardiaz, M. W. van der Kamp, A. J. Mulholland, T. E. Schrader, A. Osterman, M. P. Blakeley, P. C. E. Moody and E. L. Raven, Visualizing the protons in a metalloenzyme electron proton transfer pathway, *Proc. Natl. Acad. Sci.*, 2020, **117**, 6484–6490.

31 N. Yano, T. Kondo, K. Kusaka, T. Arakawa, T. Sakamoto and S. Fushinobu, Charge neutralization and β-elimination cleavage mechanism of family 42 L-rhamnose-α-1,4-D-glucuronate lyase revealed using neutron crystallography, *J. Biol. Chem.*, 2024, **300**, 105774.

32 Q. Wan and B. C. Bennett, "Seeing is believing": how neutron crystallography informs mechanisms by visualizing unique water species, *Biology*, 2024, **13**, 850.

33 M. T. Banco, V. Mishra, A. Ostermann, T. E. Schrader, G. B. Evans, A. Y. Kovalevsky and D. R. Ronning, Neutron structures of the Helicobacter pylori 5′-methylthioadenosine nucleosidase highlight proton sharing and protonation states, *Proc. Natl. Acad. Sci.*, 2016, **113**, 13756–13761.

34 O. Gerlits, K. L. Weiss, M. P. Blakeley, G. Veglia, S. S. Taylor and A. Kovalevsky, Zooming in on protons: neutron structure of protein kinase A trapped in a product complex, *Sci. Adv.*, 2019, **5**, eaav0482.

35 D. W. Kneller, G. Phillips, K. L. Weiss, S. Pant, Q. Zhang, H. M. O'Neill, L. Coates and A. Kovalevsky, Unusual zwitterionic catalytic site of SARS-CoV-2 main protease revealed by neutron crystallography, *J. Biol. Chem.*, 2020, **295**, 17365–17373.

36 V. N. Drago, C. Campos, M. Hooper, A. Collins, O. Gerlits, K. L. Weiss, M. P. Blakeley, R. S. Phillips and A. Kovalevsky, Revealing protonation states and tracking substrate in serine hydroxymethyltransferase with room-temperature X-ray and neutron crystallography, *Commun. Chem.*, 2023, **6**, 162.

37 V. N. Drago, R. S. Phillips and A. Kovalevsky, Universality of critical active site glutamate as an acid-base catalyst in serine hydroxymethyltransferase function, *Chem. Sci.*, 2024, **15**, 12827–12844.

38 V. N. Drago, M. P. Blakeley, R. S. Phillips and A. Kovalevsky, Revealing atomic details of pyridoxal-5′-phosphate-free and glycine external aldimine-bound serine hydroxymethyltransferase with neutron diffraction, *FEBS J.*, 2026, **293**, 582–597.

39 D. M. E. Szebenyi, F. N. Musayev, M. L. di Salvo, M. K. Safo and V. Schirch, Serine hydroxymethyltransferase: Role of Glu75 and evidence that serine is cleaved by a retroaldol mechanism, *Biochemistry*, 2004, **43**, 6865–6876.

40 J. V. K. Rao, V. Prakash, N. A. Rao and H. S. Savithri, The role of Glu74 and Tyr82 in the reaction catalyzed by sheep liver cytosolic serine hydroxymethyltransferase, *Eur. J. Biochem.*, 2000, **267**, 5967–5976.

41 V. Rajaram, B. S. Bhavani, P. Kaul, V. Prakash, N. A. Rao, H. S. Savithri and M. R. N. Murthy, Structure determination and biochemical studies on Bacillus stearothermophilus E53Q serine hydroxymethyltransferase and its complexes provide insights on function and enzyme memory, *FEBS J.*, 2007, **274**, 4148–4160.

42 S. Dajnowicz, R. C. Johnston, J. M. Parks, M. P. Blakeley, D. A. Keen, K. L. Weiss, O. Gerlits, A. Kovalevsky and T. C. Mueser, Direct visualization of critical hydrogen atoms in a pyridoxal 5′-phosphate enzyme, *Nat. Commun.*, 2017, **8**, 955.

43 J. Catazaro, A. Caprez, A. Guru, D. Swanson and R. Powers, Functional evolution of PLP-dependent enzymes based on active-site structural similarities, *Proteins*, 2014, **82**, 2597–2608.

44 K. Fesko, D. Suplatov and V. Svedas, Bioinformatic analysis of the fold type I PLP-dependent enzymes reveals determinants of reaction specificity in L-threonine aldolase from Aeromonas jandaei, *FEBS Open Bio*, 2018, **8**, 1013–1028.

45 V. N. Drago, S. Dajnowicz, J. M. Parks, M. P. Blakeley, D. A. Keen, N. Coquelle, K. L. Weiss, O. Gerlits,

A. Kovalevsky and T. C. Mueser, An N···H···N low-barrier hydrogen bond preorganizes the catalytic site of aspartate aminotransferase to facilitate the second half-reaction, *Chem. Sci.*, 2022, **13**, 10057.

46 V. N. Drago, J. M. Devos, M. P. Blakeley, V. T. Forsyth, J. M. Parks, A. Kovalevsky and T. C. Mueser, Neutron diffraction from a microgravity-grown crystal reveals the active site hydrogens of the internal aldimine form of tryptophan synthase, *Cell Rep. Phys. Sci.*, 2024, **5**, 101827.

47 M. D. Winn, C. C. Ballard, K. D. Cowtan, E. J. Dodson, P. Emsley, P. R. Evans, R. M. Keegan, E. B. Krissinel, A. G. W. Leslie, A. McCoy, S. J. McNicholas, G. N. Murshudov, N. S. Pannu, E. A. Potterton, H. R. Powell, R. J. Read, A. Vagin and K. S. Wilson, Overview of the CCP4 suite and current developments, *Acta Crystallogr., Sect. D:Biol. Crystallogr.*, 2011, **67**, 235–242.

48 P. R. Evans and G. N. Murshudov, How good are my data and what is the resolution?, *Acta Crystallogr., Sect. D:Biol. Crystallogr.*, 2013, **69**, 1204–1214.

49 A. J. McCoy, R. W. Grosse-Kunstleve, P. D. Adams, M. D. Winn, L. C. Storoni and R. J. Read, Phaser crystallographic software, *J. Appl. Crystallogr.*, 2007, **40**, 658–674.

50 P. D. Adams, P. V. Afonine, G. Bunkoczi, V. B. Chen, I. W. Davis, N. Echols, J. J. Headd, L.-W. Hung, G. J. Kapral, R. W. Grosse-Kunstleve, A. J. McCoy, N. W. Moriarty, R. Oeffner, R. J. Read, D. C. Richardson, J. S. Richardson, T. C. Terwilliger and P. H. Zwart, PHENIX: a comprehensive Python-based system for macromolecular structure solution, *Acta Crystallogr., Sect. D:Biol. Crystallogr.*, 2010, **66**, 213–221.

51 D. Liebschner, P. V. Afonine, M. L. Baker, G. Bunkoczi, V. B. Chen, T. I. Croll, B. Hintze, L. W. Hung, S. Jain, A. J. McCoy, N. W. Moriarty, R. D. Oeffner, B. K. Poon, M. G. Prisant, R. J. Read, J. S. Richardson, D. C. Richardson, M. D. Sammito, O. V. Sobolev, D. H. Stockwell, T. C. Terwilliger, A. G. Urzhumtsev, L. L. Videau, C. J. Williams and P. D. Adams, Macromolecular structure determination using X-rays, neutrons and electrons: recent developments in Phenix, *Acta Crystallogr., Sect. D:Biol. Crystallogr.*, 2019, **75**, 861–877.

52 N. W. Moriarty, R. W. Grosse-Kunstleve and P. D. Adams, electronic Ligand Builder and Optimization Workbench (eLBOW): a tool for ligand coordinate and restraint generation, *Acta Crystallogr., Sect. D:Biol. Crystallogr.*, 2009, **65**, 1074–1080.

53 M. J. Frisch, G. W. Trucks, H. B. Schlegel, G. E. Scuseria, M. A. Robb, J. R. Cheeseman, G. Scalmani, V. Barone, G. A. Petersson, H. Nakatsuji, X. Li, M. Caricato, A. V. Marenich, J. Bloino, B. G. Janesko, R. Gomperts, B. Mennucci, H. P. Hratchian, J. V. Ortiz, A. F. Izmaylov, J. L. Sonnenberg, D. Williams-Young, F. Ding, F. Lipparini, F. Egidi, J. Goings, B. Peng, A. Petrone, T. Henderson, D. Ranasinghe, V. G. Zakrzewski, J. Gao, N. Rega, G. Zheng, W. Liang, M. Hada, M. Ehara, K. Toyota, R. Fukuda, J. Hasegawa, M. Ishida, T. Nakajima, Y. Honda, O. Kitao, H. Nakai, T. Vreven, K. Throssell, J. A. Montgomery, J. E. Peralta, F. Ogliaro, M. J. Bearpark, J. J. Heyd, E. N. Brothers, K. N. Kudin, V. N. Staroverov, T. A. Keith, R. Kobayashi, J. Normand, K. Raghavachari, A. P. Rendell, J. C. Burant, S. S. Iyengar, J. Tomasi, M. Cossi, J. M. Millam, M. Klene, C. Adamo, R. Cammi, J. W. Ochterski, R. L. Martin, K. Morokuma, O. Farkas, J. B. Foresman and D. J. Fox, *Gaussian16 Rev. B.01*, Gaussian Inc, Wallingford, CT, 2018.

54 F. Meilleur, P. Munshi, L. Robertson, A. D. Stoica, L. Crow, A. Kovalevsky, T. Koritsanszky, B. C. Chakoumakos, R. Blessing and D. A. A. Myles, The IMAGINE instrument: first neutron protein structure and new capabilities for neutron macromolecular crystallography, *Acta Crystallogr., Sect. D:Biol. Crystallogr.*, 2013, **69**, 2157–2160.

55 F. Meilleur, L. Coates, M. J. Cuneo, A. Kovalevsky and D. A. A. Myles, The neutron macromolecular crystallography instruments at Oak Ridge National Laboratory: Advances, challenges, and opportunities, *Crystals*, 2018, **8**, 388.

56 F. Meilleur, A. Kovalevsky and D. A. A. Myles, IMAGINE: The neutron protein crystallography beamline at the high flux isotope reactor, *Methods Enzymol.*, 2020, **634**, 69–85.

57 J. W. Campbell, Lauegen, an X-Windows-Based Program for the Processing of Laue X-Ray-Diffraction Data, *J. Appl. Crystallogr.*, 1995, **28**, 228–236.

58 J. W. Campbell, Q. Hao, M. M. Harding, N. D. Nguti and C. Wilkinson, LAUEGEN version 6.0 and INTLDM, *J. Appl. Crystallogr.*, 1998, **31**, 496–502.

59 S. Arzt, J. W. Campbell, M. M. Harding, Q. Hao and J. R. Helliwell, LSCALE - the new normalization, scaling and absorption correction program in the Daresbury Laue software suite, *J. Appl. Crystallogr.*, 1999, **32**, 554–562.

60 M. Weiss, Global indicators of X-ray data quality, *J. Appl. Crystallogr.*, 2001, **34**, 130–135.

61 M. Mustyakimov and P. Langan, *nCNS: an Open Source Distribution Patch for CNS for Macromolecular Structure Refinement*, Los Alamos National Security, Los Alamos, NM, USA, 2007.

62 P. D. Adams, M. Mustyakimov, P. V. Afonine and P. Langan, Generalized X-ray and neutron crystallographic analysis: more accurate and complete structures for biological macromolecules, *Acta Crystallogr., Sect. D:Biol. Crystallogr.*, 2009, **65**, 567–573.

63 A. T. Brunger, P. D. Adams, G. M. Clore, W. L. DeLano, P. Gros, R. W. Grosse-Kunstleve, J. S. Jiang, J. Kuszewski, M. Nilges, N. S. Pannu, R. J. Read, L. M. Rice, T. Simonson and G. L. Warren, Crystallography & NMR system: A new software suite for macromolecular structure determination, *Acta Crystallogr., Sect. D:Biol. Crystallogr.*, 1998, **54**, 905–921.

64 A. Casanal, B. Lohkamp and P. Emsley, Current developments in Coot for macromolecular model building of Electron Cryo-microscopy and Crystallographic Data, *Protein Sci.*, 2020, **29**, 1069–1078.

65 (*a*) 10 YN, 2026; (*b*) 10 ZB, 2026.